Journal of CO2 Utilization 54 (2021) 101796

Contents lists available at ScienceDirect

Journal of CO2 Utilization

journal homepage: www.elsevier.com/locate/jcou

Exploring Cu_xO-doped TiO_2 modified with carbon nanotubes for CO_2 photoreduction in a 2D-flow reactor

J. Fernández-Catalá, M. Navlani-García, Á. Berenguer-Murcia, D. Cazorla-Amorós *

Materials Science Institute and Inorganic Chemistry Department, University of Alicante, Ap. 99, E-03080 Alicante, Spain

ARTICLE INFO

Keywords:
Photocatalysis
CO_2
CH_4
Z-scheme
Flow reactor

ABSTRACT

Different photocatalysts based on the combination of TiO_2 and Cu_xO have been prepared by simple and reproducible procedures. The synthesized systems have been applied in the photoreduction of CO_2 to yield CH_4 inside a 2-dimensional flow reactor in which the gas stream was passed over a thin layer of the catalyst under UV irradiation. Analysis of the photocatalysts reveals that the oxidation state of Cu changes throughout the reaction, thus modifying the physicochemical properties of the catalysts. The combination of core-level and valence-band level spectroscopies allowed us to draw the band diagram for the best catalyst, showing a Z-scheme structure. The reactor design and the photocatalyst developed can produce CH_4 at a very high production rate with extreme efficiency. After further optimization through suppression of side reactions, we obtained one of the highest values reported for any type of reactor or catalytic system with a CH_4 formation rate over 100 $\mu mol_{CH4} \cdot g_{cat}^{-1} h^{-1}$ using low power LED lighting.

1. Introduction

Climate change is directly linked to the use of fossil fuels to meet current energy demand which is currently estimated at 400 EJ worldwide [1]. This has spurred research towards the development of catalytic routes and processes aimed at the production of clean energy. The ultimate goal is the exploration into new catalytic reactions in which wastes are converted to useful products [2–4]. In this respect, the reduction of CO_2 into useful chemicals appears as an ideal solution. The Sun provides Earth with 5.5×10^6 EJ worth of solar energy per year globally [5]. Thus, photocatalytic reactions hold a very high potential for their use in energy-related research [6,7]. Under these particular optics the development of photocatalysts capable of harnessing light and use it for the production of fuels is both exciting and necessary from a global environmental viewpoint.

The process of reducing CO_2 by means of a photocatalyst under sunlight irradiation is a term often referred to as "artificial photosynthesis" [8]. The main reaction products of significant interest from an industrial viewpoint (primarily CH_4, CO and CH_3OH) is still far below the expected outcome. Thus, substantial breakthroughs are mandatory in several aspects, especially in catalyst formulation and design as well as in reactor architecture.

Over the past decade, extensive research has been carried out to modify existing photocatalysts to improve desired product yields so as to make photocatalysis a viable route towards a circular economy. TiO_2 is by far the most widely studied photocatalyst since its photocatalytic properties were established in 1972 by Fujishima and Honda [9]. However, it is not devoid drawbacks, such as high electron-hole recombination rate, relatively low surface area, and very low activity under solar irradiation [10]. All these would ultimately make its use in artificial photosynthesis unfeasible. For these reasons, the key aspects which have been tackled in the literature are the modification of absorption of light in the visible region of the spectrum or to modulate the rate of electron-hole pairs recombination [5,10,11]. In this respect, many reports may be found in which noble metals (e.g. Au, Ag, Pd or Rh) have been used in combination with TiO_2-based systems. Nevertheless, the results obtained do not make up for the increase in photocatalyst cost [12]. In this sense, the use of other cheaper and more abundant transition metal-based catalysts is highly desirable [13–15]. The formation of Cu_xO and TiO_2 hybrids has given rise to a new family of photocatalysts often referred to in the literature as Z-scheme heterostructures or Z-scheme photocatalysts. In these systems, two different semiconductors are linked so as to work together in a given photocatalytic reaction. Z-scheme heterostructures combine the benefits of both materials, preserving both strongly oxidative holes and strongly reducing electrons [16–18]. In these heterostructures, the interface between the oxides is

* Corresponding author.
E-mail address: cazorla@ua.es (D. Cazorla-Amorós).

https://doi.org/10.1016/j.jcou.2021.101796
Received 23 September 2021; Received in revised form 25 October 2021; Accepted 30 October 2021
Available online 8 November 2021
2212-9820/© 2021 The Author(s). Published by Elsevier Ltd. This is an open access article under the CC BY-NC-ND license (http://creativecommons.org/licenses/by-nc-nd/4.0/).

crucial in establishing the performance of the photocatalyst. Thus, special attention must be paid to the development and analysis of this particular aspect [19]. Also, another interesting alternative to improve the photocatalytic activity of TiO_2 is the incorporation of carbon materials [20]. In this sense, the use of carbon nanotubes (CNTs) has attracted a significant attention for their incorporation on the TiO_2 due to their interesting properties. CNTs enhance the lifetime of generated electron-hole (e^--h^+) pairs in the TiO_2 and they can provide supplementary catalytic active sites under certain reaction conditions, among other benefits [21,22]. In this study, taking profit of the electrical properties of CNTs, a CNTs film has been prepared and the two metal-based phases have been loaded separately in order to deepen into the reaction mechanism.

Another key aspect which must be addressed when improving upon a (photo)catalyst lies in the understanding of the mechanism of CO_2 photoreduction [23]. The reaction steps at the atomic/molecular level are still not well understood and thus subject to discussion [24,25]. It is generally accepted that the reaction pathways involve the following steps: (1) reactants adsorption on the surface of the photocatalyst, (2) activation/bond weakening of the adsorbed reactants by electrons/holes generated by light irradiation, (3) generation of reactions intermediates on the photocatalyst surface, (4) formation of reaction products, and (5) catalyst surface regeneration [26]. Considering the photocatalysis reactor, the lack of an established and generally accepted standard has resulted in the development of custom-built photoreactor set-ups. In these reactors working conditions and products distributions is monitored according to the needs/parameters of each laboratory. This has resulted in an inherent difficulty in comparing the performance of the samples which have been tested in different facilities. The photoreduction of CO_2 may be performed both in liquid and gas phases [4,27,28]. The former configuration is strongly dominated by slurry reactors [29–31]. Nevertheless, the use of a gas-phase reaction system bears a significant number of advantages over liquid-phase reactors, out of which the following stand out: (1) the possibility of operating in very well controlled high-purity conditions, and (2) the fact that dissolution phenomena arising from the presence of water as hydrogen source (which can moreover be perfectly controlled) may be safely ruled out [32].

Focusing on gas-phase reactions, batch mode reactors are often used [33,34]. This raises the question of whether product accumulation and/or intermediates or products readsorption may give rise to other secondary or competing reactions. Thus, it becomes preferable to perform CO_2 photoreduction in a continuous flow reactor. This is done by supplying CO_2 and H_2O (steam) with short yet controlled contact times between the catalyst and the gas phase. Under these conditions, while the aforementioned deleterious effects might occur to a lesser or negligible extent, the very small amounts of products generated require appropriate reactor design and data analysis in order to deliver meaningful and reliable results. This must be considered together with the fact that light penetration in these systems goes to depths well below 0.5 μm (for instance, radiation with a wavelength of 355 nm will penetrate under 300 nm into anatase TiO_2 [35]). Thus, appropriate reactor design becomes yet another cornerstone to bear in mind. The reactor architectures that have been described in the few literature reports available are based on a thin bed of photocatalyst loaded inside a selected reactor chamber. The reactor is submitted to continuous radiation while CO_2 and H_2O are fed during the reaction. These may be divided into (1) a "flow-over" (or "flow-through") reactor in which a thin layer of the photocatalyst is deposited on a flat transparent substrate while the reaction mixture is passed over (or through) the bed [36], and (2) a thin tubular reactor with a small cross-section in which the catalyst is loaded as a packed bed constantly illuminated as the gas mixture flows through it [37].

The objective of the present work is to prepare a series of photocatalysts based on the combination of TiO_2 and Cu_xO, in order to develop high-performance Z-scheme systems. The prepared samples were analyzed by several physical and chemical techniques to probe into their structure and the nature of the interface between the semiconductors. Finally, the photocatalysts were tested in the photoreduction of CO_2 in a flow reactor that uses a thin layer of the photocatalyst, thus being considered as a 2-dimensional flow reactor. The device is designed to irradiate the sample with UV LED lights during the experiments. Our results show that it is possible to develop efficient Z-scheme photocatalysts which can operate under steady state conditions, which would allow to deliver a promising amount of CH_4 in a gas stream. Some insights into the reaction mechanism have been obtained with the help of CNTs as charge carrier for metal oxides phase separation.

2. Experimental

2.1. Reagents and materials

Titanium (IV) butoxide (TTB, 97 %, Sigma-Aldrich), Multi-walled Carbon Nanotubes (MWCNT, Nanoblack, bamboo-type MWCNT with a diameter between 15 and 30 nm), glacial acetic acid (HAc, 99 %, Sigma-Aldrich), Pluronic F-127 (F-127, Sigma-Aldrich), absolute ethanol (EtOH, 99.8 %, Fisher Scientific), formamide (FA, 99.5 %, Sigma-Aldrich), urea (99 %, Merck), copper nitrate trihydrate ($Cu(NO_3)_2{\cdot}3H_2O$, 99 %, Panreac), sodium borohydride ($NaBH_4$, 98 %, Sigma-Aldrich), methanol (MeOH, 99.8 %, Sigma-Aldrich), glass plates (24 × 24 mm, Thermo Scientific Menzel, Fisher Scientific), commercial TiO_2 (P25, Rutile:Anatase 85:15, 99.9 %, Degussa) and deionized water were used in the present work. All reactants were used as received, without further purification.

2.2. Catalyst preparation

2.2.1. Synthesis of TiO_2 and their modification with MWCNT

The base TiO_2 used in all the preparations and its composite with MWCNT was synthesized following the preparation protocol reported by our research group [38,39]. For the benchmark TiO_2, 5 g of the titanium precursor (TTB) were dissolved in a small amount (7.9 g) of EtOH. The resulting solution (labelled "Solution A") was vigorously stirred for 10 min. In a separate vessel 1.6 g of HAc, 0.3 g of Pluronic F-127, 1.6 g of H_2O, 7.9 g EtOH, 0.4 g of FA, and 0.4 g of urea were mixed (this container was labelled "Solution B") and stirred for 10 min. After the stirring period was finished "Solution B" was added dropwise to "Solution A" under strong magnetic stirring. The obtained solution was quickly transferred to a Teflon-lined stainless-steel autoclave and heated at 60 °C for 24 h to promote the formation of the TiO_2 gel. The temperature was then increased to 120 °C for 24 h to promote the decomposition of urea. The obtained white solid was calcined at 350 °C to remove the template. For the preparation of the TiO_2-MWCNT composites, the necessary amount of MWCNTs to yield a 1 wt. % in the final composite was added to "Solution B" following the same synthetic protocol. The MWCNTs were then dispersed in "Solution B" by means of an ultrasound probe (Bandelin SONOPULS HD 2200) with a power of 660 W operating at 30 % power for 5 min. Following this step, the synthesis was carried out under the same aforementioned conditions for the support based on bare TiO_2. The resulting materials were denoted as TiO_2 for the sol-gel titania, TiO_2C for the TiO_2-MWCNT composites. "P25" refers to the benchmark P25 used as reference.

2.2.2. Synthesis of Cu-containing photocatalysts

The impregnation of a transition metal (Cu) on the surface of TiO_2, TiO_2C, and P25 was carried out by a modification of a standard impregnation protocol followed by a reduction step with $NaBH_4$ [40]. Firstly, 500 mg of the starting material (TiO_2, TiO_2C or P25) were suspended in 10 mL of deionized water, using an ultrasound bath for 5 min. After that, the necessary amount of a solution of the metal precursor (1.9 g/200 mL) was added to obtain a final metal loading of 1 wt. %. This suspension containing the precursor was stirred for 1 h. Then, the Cu

ions were reduced by incorporation of a freshly prepared $NaBH_4$ aqueous solution (molar ratio between metal and $NaBH_4$ was 1:10) dropwise to the suspensions under vigorous stirring and the resulting mixture was stirred for 1 h. Finally, the powder was filtered and washed with an ethanol:water mixture three times to totally remove the remaining $NaBH_4$ present in the samples. The photocatalysts were dried at 60 °C for 12 h. In the case of TiO_2C photocatalyst, different Cu loadings (1, 2, and 5 wt. %) were prepared by the same procedure. The prepared Cu-containing photocatalysts were named as (Cu_xTiO_2C, Cu_1TiO_2 and Cu_1P25) where "X" corresponds to the nominal Cu loading used for each sample, "TiO_2" stands for our synthesized TiO_2, "C" corresponds to the MWCNTs, and "P25" stands for P25 titania.

2.2.3. Preparation of active phase (Cu_xO and/or TiO_2) supported on MWCNT film

To study the interplay between the TiO_2 phase and the Cu_xO phases and its effect in the overall performance of the resulting photocatalysts, a series of samples was prepared. First a film of MWCNT was prepared by mixing 95 wt. % of the MWCNT and 5 wt.% polytetrafluoroethylene (PTFE) binder solution (Sigma Aldrich). This sample was named MWCNT film. With this objective the photocatalyst TiO_2 and Cu_xO have been deposited on the previously prepared MWCNT film using three different approaches:

1) MWCNT film with Cu: To incorporate Cu_xO on the surface of the MWCNT film, the film was immersed partially in an aqueous Cu $(NO_3)_2$ solution (1.9 g/200 mL) for 5 min three times. After the dipping stage, the plate was dried at 60 °C overnight. The sample was named MWCNT film w/ Cu
2) MWCNT film with P25: To incorporate TiO_2 on the surface of MWCNT film, a small amount of P25 was deposited as a thin layer on the surface of MWCNT film. The sample was named MWCNT film w/ P25.
3) MWCNT film with P25 and Cu: In this sample, Cu_xO and TiO_2 were incorporated one on each side of the film without being in contact, following the deposition methodologies of approaches 1 and 2. The sample was named MWCNT film w/ P25&Cu.

2.3. Catalyst characterization

The crystallinity of the samples was determined by X-ray diffraction (XRD) analysis using a Miniflex II Rigaku apparatus using Cu Kα radiation and a scanning rate of 1°/min, in the 2θ range 6−80°.

The morphology analysis of the materials was performed by transmission electron microscopy (TEM, JEOL JEM 2010) and field-emission scanning electron microscope (FE-SEM, ZEISS, Merlin VP Compact).

The metal (Cu) loading present in the catalysts was analyzed by inductively coupled plasma emission spectroscopy (ICP-OES) using a Perkin-Elmer Optima 4300 system. Dissolution of the different catalysts was carried out by treating them with HF at room temperature, in order to ensure the total dissolution of the samples.

The amount of MWCNTs in the composites (TiO_2C) was obtained from the weight loss in the 450−600 °C interval measured by thermogravimetric analysis (TG analysis) using a thermobalance (SDT 2960). The sample was heated up to 900 °C in air, using a heating rate of 5 °C min^{-1} in the aforementioned equipment.

In situ UV–vis spectra were collected with a Flame UV–vis Spectrometer (Ocean optics) using a deuterium halogen source (Avantes, DH-2000). The absorbance of the materials was measured in the range of 200 nm–800 nm using $BaSO_4$ as background. To perform the in situ UV–vis spectra the most interesting catalysts for the photoreduction of CO_2 were incorporated on the surface of a glass plate (24 × 24) mm and introduced in the flow reactor. Then, the reagents (CO_2 and water vapor) were passed through the reactor. The UV light was then turned on to perform the reaction under the same conditions as those described for the catalytic test (see Section 2.4. "Photocatalytic tests", vide infra). UV–vis spectra were recorded every 10 min in order to evaluate the evolution of the absorbance properties (UV and Visible range) of the catalysts during reaction. These measurements were also performed on all the fresh catalysts prepared in this work to study their absorbance properties.

X-ray Photoelectron Spectroscopy (XPS) was performed using a K-α spectrometer from Thermo-Scientific, equipped with an Al anode. UPS analyses were conducted in an integrated ultrahigh vacuum system, connected to an automated Nexsa spectrometer (Thermo scientific). UPS spectra were obtained using the first of the two resonance lines from a He lamp (He I ($h\nu = 21.2$ eV)). In order separate the secondary edges of the sample and analyzer, a negative potential of about 9.3 V was applied to the sample. Prior to measurements, an Ag foil was cleaned by argon ion sputtering. The bias was optimized to shift the Ag spectrum in the linear region of the analyzer (0–10 eV kinetic energy). A work function for the silver reference of 4.2 eV was obtained, in good agreement with the literature [41].

2.4. Photocatalytic tests

The performance of the prepared photocatalysts in the reduction of CO_2 in the presence of water vapor to yield CH_4 using a flow reactor was evaluated under ambient conditions as follows in the set-up depicted in Scheme 1: 40 mg of the catalyst were incorporated as a thin layer on the surface of a glass plate (24 × 24) mm. The glass plate with the catalyst was introduced inside a metal casing which was designed to operate in a flow-over regime. The catalyst was purged using a stream of pure CO_2 (99.999 %) with a flow of 5 mL/min passing through the reactor until steady state was reached (12 h). Then, water vapor was incorporated in the pure CO_2 stream using a water bubbler (30 ± 2.0 °C giving a water vapor pressure of 0.0418 bar) to saturate the stream of CO_2 with H_2O until steady state was once again reached (1 h). Finally, the catalyst was irradiated with a UV LED light (combined power output 1 W) with a wavelength of 365 nm at room temperature to perform the reduction of CO_2 to fuels. Additionally, blank tests were performed under the same experimental conditions as the catalytic tests and no catalytic activity was detected in the absence of photocatalyst. Namely, these conditions comprised performing the reaction under standard conditions in the absence of photocatalyst using CO_2/H_2O/UV light and in the presence of photocatalyst using He/H_2O/UV light. Other products such as higher hydrocarbons (C_{2+}) or CO were also analyzed for their presence during the photoreaction and were always in very small amounts (<1 %). Analysis of the samples was carried out by gas chromatography (GC) in an Agilent 6890 N chromatograph working with a CTR-I column at 70 °C to separate the products, sub-products and reagents using two detectors (flame ionization detector (FID) and a TCD) to analyze the products of the reaction. The catalytic test of the sample was analyzed every 10 min in the GC for 4 h of the reaction. Also, in this study we measured the samples in film configuration (see Section 2.2.3) to address the interplay between the TiO_2 phase and the Cu_xO phases and its effect in the overall performance of the resulting photocatalysts. In this sense the samples with the bare MWCNT film (sample MWCNT film), MWCNT film with Cu (sample MWCNT film w/ Cu), MWCNT film with P25 (sample MWCNT film w/ P25), MWCNT film with P25 and Cu (sample MWCNT film w/ P25&Cu), and MWCNT film with P25 and shielded Cu (sample MWCNT film w/ P25&sCu) were analyzed. In this latter sample the Cu phase was shielded using aluminum foil to prevent any irradiation from the UV source and it was analyzed using the same condition described previously in this section.

3. Results and discussion

3.1. Pre-reaction

X-Ray diffraction was firstly used to establish the crystalline phases present in the samples. The results (Fig. 1) clearly show that the TiO_2

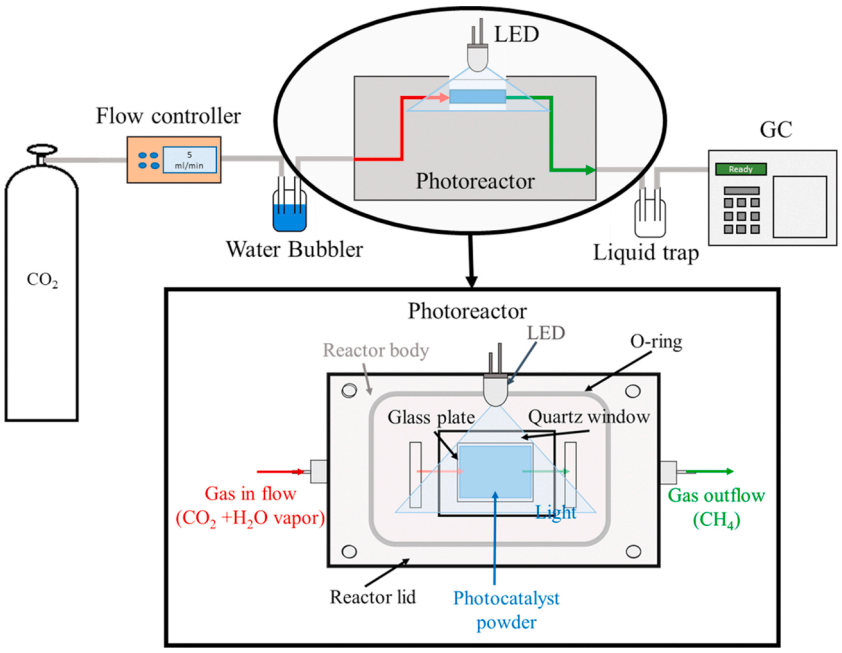

Scheme 1. Illustration of the experimental setup and photoreactor design used for CO_2 photoreduction catalytic tests.

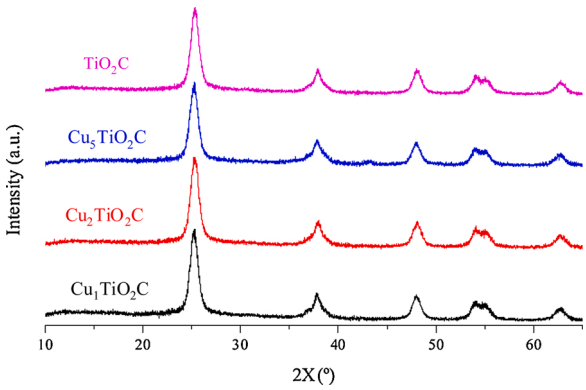

Fig. 1. XRD patterns of the catalysts prepared in this study.

samples synthesized in all the prepared samples present the characteristic peaks of the anatase phase, while those samples prepared using P25 had a Rutile:Anatase ratio 85:15 according to the characteristics specified by the supplier [38,40]. Given their absence of long-range order, MWCNTs did not show in the diffractogram. Concerning the Cu-containing samples, the only XRD pattern which denoted the presence of any Cu phases were those of samples with the highest loading (5 wt.%), in which a very weak and broad peak was apparent at a diffraction angle 42.5° which corresponds to standard Cu_2O [42,43] (JPPDS no. 05-0667). Our results indicate that all Cu-based catalysts contained very small nanoparticles in the range of a few nanometers in amounts that could not be detected by means of XRD, even though other techniques such as electron microscopy clearly showed the presence of such species (see below).

In order to get a better idea of the morphology as well as the contact between the different components of the prepared systems, transmission electron microscopy was performed on all the samples. The binary systems (Cu_1P25 and Cu_1TiO_2) showed clear differences between the two TiO_2 phases. In the former, well-defined polygonal crystals with a size between 10 and 60 nm were dominant, whereas in the latter the TiO_2 grains showed a predominance of irregular shaped grains with sizes which went down to 5 nm. This clearly reflects the difference in the synthetic procedure for both oxides, being pyrolysis the method for commercial P25, while sol-gel followed by calcination at 350 °C was the method employed in the synthesis of as-synthesized TiO_2 sample. Another distinct feature of the two samples is the fact that while in the case of the Cu_1P25 sample the deposited Cu-based nanoparticles are clearly visible all over the surface of the well-defined TiO_2 crystals with an average size of approximately 2 nm (See Fig. 2B), in the Cu_1TiO_2 sample the same synthetic protocol renders Cu-based species which are practically undiscernible by TEM, even though ICP data (see below) clearly revealed the presence of a very similar amount of Cu in both samples.

Concerning the ternary systems (Cu_XTiO_2C), the images shown in Fig. 3 illustrate how the MWCNTs are well integrated and present an intimate contact with the Cu-decorated TiO_2 particles for all the Cu loadings studied. It must be noted that at high loadings the presence of Cu aggregates could also be observed using TEM imaging, in agreement with our XRD results.

In order to verify that the intended amounts of Cu were successfully loaded on the catalysts, the samples were dissolved in HF and analyzed by ICP-OES. Table 1 shows that all samples contained Cu amounts that were very close to the nominal loading.

UV–vis spectroscopy was performed in all samples before reaction in order to determine not only the potential response of the synthesized samples under UV–vis light (Fig. 4), but also to establish the coordination and geometry of the TiO_2 species present in our samples, as we have reported earlier [13]. Concerning the latter, all samples showed very strong UV absorption in the 250−400 nm range, which was a clear indicative of Ti in octahedral coordination. In terms of absorption in the visible range, noticeable differences were observed depending on the sample. While pure TiO_2-based samples showed negligible absorption at wavelengths above 400 nm, the samples containing Cu displayed a very broad band from 550 nm to 850 nm due to Cu_xO phases [44]. Furthermore, Cu deposition also results in the formation of an interfacial charge transfer between the TiO_2 and the Cu species, resulting in a small extension of the absorption range $\lambda = 400-430$ nm [12,45]. The most noticeable differences were observed for the MWCNT-containing samples, where even a small amount of carbon nanotubes in the sample (1 wt. %) yielded a very high absorption in the whole visible range. From the analysis of the UV spectra the band gap energy for each sample was calculated and presented in Table 2.

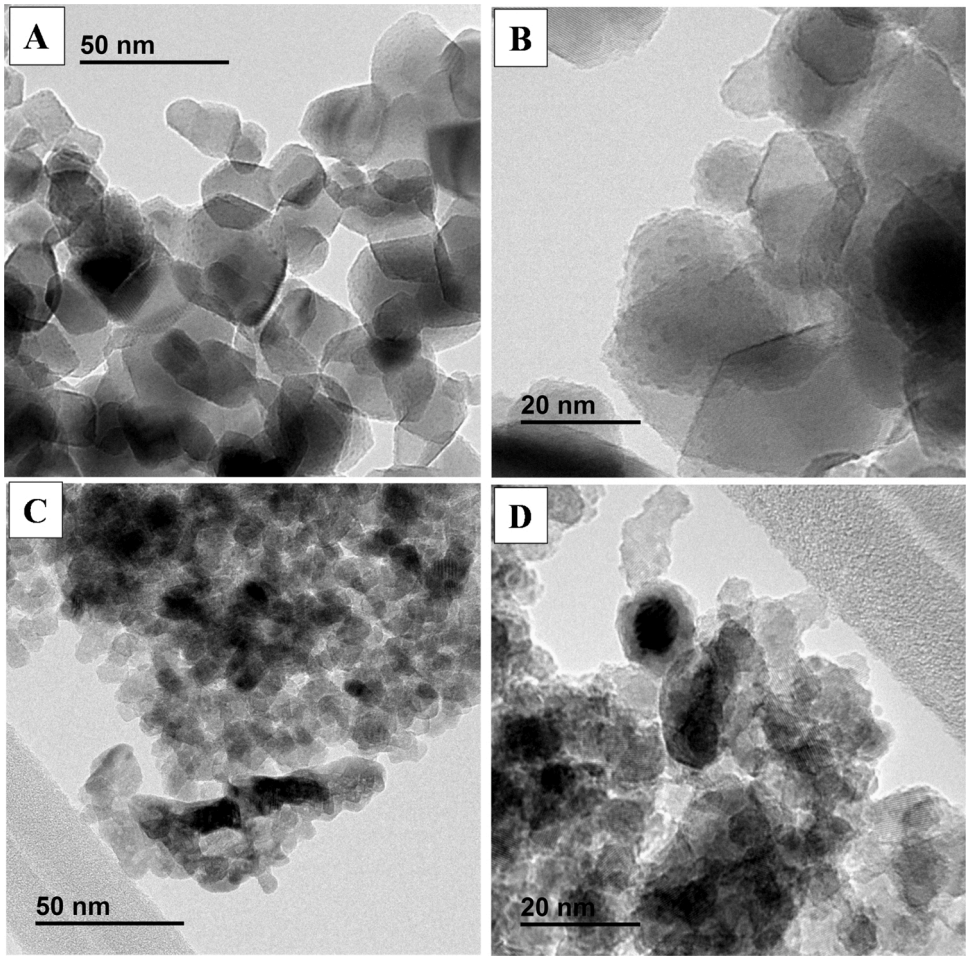

Fig. 2. TEM micrographs of the binary photocatalysts: (A) and (B) sample Cu_1P25 and (C) and (D) sample Cu_1TiO_2.

3.2. Reaction

The photocatalytic CO_2 reduction tests performed on the different samples prepared in this work yielded CH_4 as the major product, with trace amounts of CO were present in the effluent stream. The CH_4 formation rate (in $\mu mol_{CH4} \cdot g_{cat}^{-1}\ h^{-1}$) after 4 h of reaction is shown in Fig. 5. The results indicate that bareTiO_2 (either P25 or the TiO_2 synthesized in this work) perform similarly, with the P25 edging ahead. The addition of MWCNTs appeared to hinder the formation of CH_4 since the formation rate dropped just below 0.1 $\mu mol_{CH4} \cdot g_{cat}^{-1}\ h^{-1}$. From our previous results [39], we would have expected the addition of MWCNTs to exert a positive influence on the formation of CH_4 since their presence enhances the lifetime of electron-hole pairs, but our results showed that it was not the case. The picture changed significantly with the addition of Cu to the P25 and TiO_2 (Cu_1P25 and Cu_1TiO_2) samples. In this case, while both samples improved compared to their Cu-free counterparts, sample Cu_1TiO_2 (containing the sol-gel TiO_2) experienced a 10-fold increase in its CH_4 formation rate, greatly surpassing the P25-based sample. In this respect, the addition of a transition metal-based phase with a marked tendency towards the formation of surface formiates/carbonates clearly yielded an improved photocatalyst over the bare TiO_2 photocatalyst [46,47]. We also explored the possibility of efficiently incorporating MWCNT into the sol-gel process, thus creating a good contact between the metal oxide phase and the carbon material. Sample Cu_1TiO_2C showed a similar (yet slightly slower) CH_4 formation rate to sample Cu_1TiO_2, indicating that the presence of MWCNTs in the sample was detrimental. In this respect, the incorporation of MWCNTs with the P25 did not give positive results since the co-suspension of both materials followed by evaporation did not yield materials with improved properties (results not shown). In this respect, the best samples presented so far in this study appeared to combine two characteristics that worked exceedingly well together:

(1) A semiconductor photocatalyst able to efficiently generate electron-hole pairs when irradiated with low-power UV light
(2) A Cu-based phase which can adsorb CO_2 and transform it into fuels with the electrons coming from either the semiconductor (directly) or the carbon material (indirectly). In the latter case, as Fig. 5 shows, the presence of the selected carbon material is slightly detrimental towards the formation of CH_4.

It must be noted that while these CH_4 production rates are amongst the highest reported values to date using similar TiO_2-based systems, the employed incident light was in the UV range. Another recent study with similar catalysts was reported by Ali et al. [12] in which they used reduced TiO_2 (RT) in conjunction with a Cu phase, which the authors identified as Cu_2O, to reduce CO_2 in a flow reactor. In their case, by using simulated solar light illumination (1 Sun), provided by a solar simulator, they observed a CH_4 formation rate of 0.077 $\mu mol_{CH4} \cdot g_{cat}^{-1}\ h^{-1}$. In our case, using UV-LED lights (combined power output 1 W) with a wavelength of 365 nm, our formation rate reached 1.136 $\mu mol_{CH4} \cdot g_{cat}^{-1}\ h^{-1}$. This alone clearly shows the outstanding potential of these systems.

However, there is one very important aspect that needs considering: all the reported results in our or any other study so far refers to the steady-state CH_4 formation rate which the authors have observed after

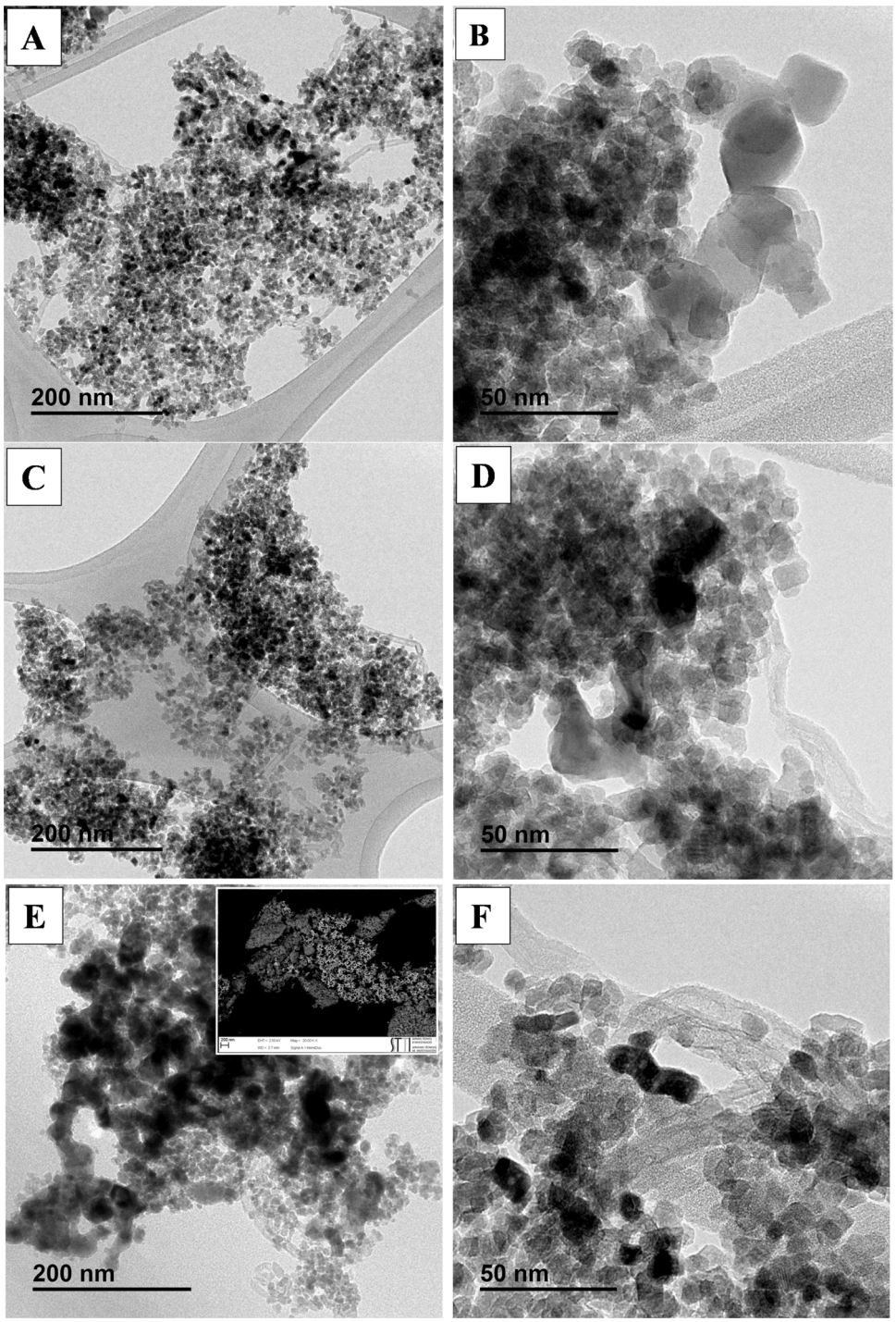

Fig. 3. TEM micrographs of the ternary photocatalysts: (A) and (B) sample Cu_1TiO_2C, (C) and (D) sample Cu_2TiO_2C, and (E) and (F) sample Cu_5TiO_2C. The inset in Fig. 3E corresponds to a FE-SEM image of the sample showing the Cu phase aggregates (right-hand side).

Table 1
Cu loadings determined by ICP-OES for the different photocatalysts.

Sample	Nominal Cu loading (wt. %)	Loading determined with ICP-OES (wt. %)
Cu_1P25	1	1.14 ± 0.02
Cu_1TiO_2	1	1.08 ± 0.01
Cu_1TiO_2C	1	1.14 ± 0.03
Cu_2TiO_2C	2	2.04 ± 0.03
Cu_5TiO_2C	5	5.07 ± 0.09

the reaction has occurred for a given timespan (typically in the range of 4–6 h to ensure a stable operational regime). However, it is often the case that the initial stages of a (photo)catalytic process may pose the greatest challenge to control but also the best opportunity to improve upon the results obtained under steady-state conditions. With this idea in mind, we monitored the CH_4 formation rate for the different catalysts over the first four hours of reaction (Fig. 6).

While the samples containing sol-gel TiO_2 (Cu_1TiO_2 and Cu_1TiO_2C) showed an initial increase over the first 20–50 min of reaction (with the sample containing carbon nanotubes reaching a plateau after approximately 30 min), the P25-based sample presented a very steep increase in

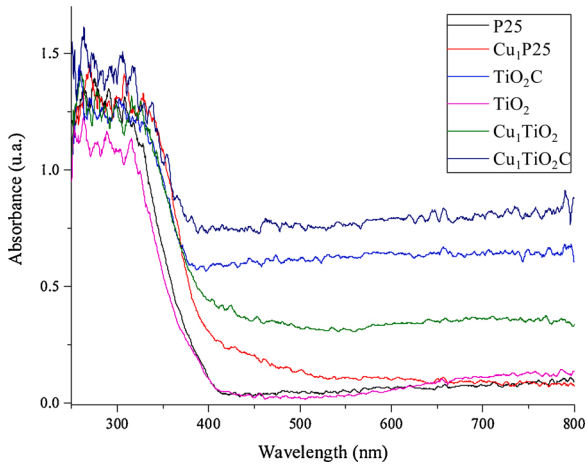

Fig. 4. UV–vis spectra of the different photocatalysts analyzed.

Table 2
Band gap energies determined from UV–vis spectra for the different photocatalysts.

Sample	E_g (eV)
P25	3.14
TiO_2	3.09
TiO_2C	2.96
Cu_1P25	3.12
Cu_1TiO_2	2.91
Cu_1TiO_2C	2.81

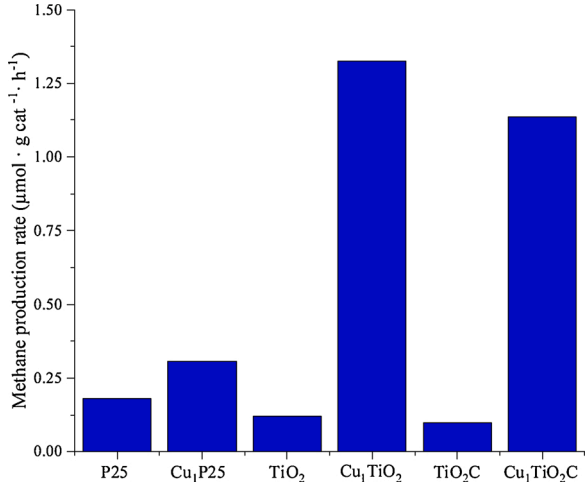

Fig. 5. CH_4 production rates for the different photocatalysts.

CH_4 formation rate at the initial stages of the reaction, followed by a similarly steep decline until reaching the observed steady-state CH_4 formation rate. This trend evidenced the existence of competing processes in the case of the Cu_1P25 which despite being negligible during the initial stages (with CH_4 formation rate values reaching 8.056 $\mu mol_{CH4} \cdot g_{cat}^{-1}\ h^{-1}$), gained enough relevance after the first 30 min to reduce the maximum observed values by almost one order of magnitude. By comparing the samples, one distinct characteristic is the presence of a carbon material in the Cu_1TiO_2C sample. Considering that the intrinsic benefit of the nanotubes acting as electron conductors between the Cu_xO phases is easily overruled by the fact that the Cu-based species are primarily located on the TiO_2 particles, the distinctive factor must arise from the fact that the carbon material acts as a hole scavenger, thus stabilizing the CH_4 formation rate in the case of the Cu_1TiO_2C sample. In

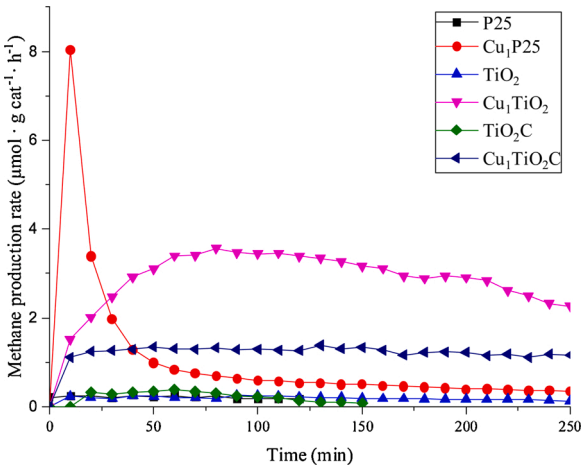

Fig. 6. Evolution of the CH_4 formation rate for the different photocatalysts analyzed in this study over several hours of reaction.

this respect, the lack of a hole scavenger plays a key detrimental role in the performance of the P25-based photocatalyst. With this in mind, a very small amount of a suitable hole scavenger (EtOH) was added to the water bubbler located before the photoreactor. After testing different amounts of scavenger (between 3 and 100 μL of EtOH), the optimum

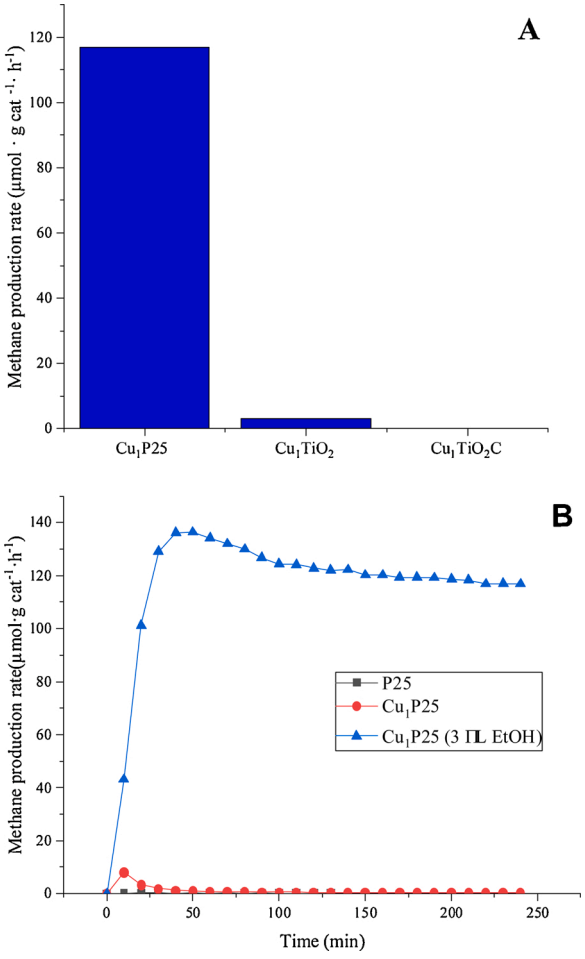

Fig. 7. (A) Steady-state CH_4 formation rates for samples Cu_1P25, Cu_1TiO_2, and Cu_1TiO_2C using ethanol as hole scavenger; (B) Evolution of the CH_4 formation rate for the best performing sample (Cu_1P) under standard reaction conditions using EtOH as hole scavenger.

amount was found to be 3 μL of EtOH in 2.5 mL of distilled H_2O. Fig. 7 shows the CH_4 formation rate for the different photocatalysts and the evolution of the CH_4 formation rate for the best performing sample.

Two very important features become obvious from these results. The first one is that in the case of the Cu_1TiO_2C, the existence of a second hole scavenger is largely detrimental. This may be either due to the two scavengers (carbon nanotubes and ethanol) competing for the neutralization of holes in the TiO_2 phase once the electron-hole pairs are formed or to the adsorption of EtOH on the surface of the carbon nanotubes, the result being in both cases an ineffective hole scavenging capacity. The second key feature is the fact that in the case of the P25-based sample, the CH_4 formation rates spiked to almost 140 $\mu mol_{CH4} \cdot g_{cat}^{-1}\ h^{-1}$, reaching a steady-state value of 117 $\mu mol_{CH4} \cdot g_{cat}^{-1}\ h^{-1}$, two orders of magnitude higher than our best result so far in this work and over three orders of magnitude higher than the best reported results using a similar system [12], highlighting the unparalleled efficiency of the Cu_1P25 system by just incorporating a very small amount of EtOH in the feed stream. It should be noted that the presence of trace amounts of C_2H_4O (the oxidation product of EtOH) was detected in the outlet stream, but its concentration was always below 1 % of the total components concentration.

In another report, a flow reaction system based on a tubular reactor system was used [37]. In this case, using a high-power UV light the highest CH_4 formation rate was 23 $nmol \cdot g_{cat}^{-1}\ h^{-1}$. Biswas et al. [48] reported the use of Cu/TiO_2 catalysts in a continuous flow reactor with a configuration similar to ours. By using a Xe arc lamp they obtained CO as the major product (over 60 $\mu mol \cdot g_{cat}^{-1}\ h^{-1}$) together with CH_4 (highest concentration was 10 $\mu mol \cdot g_{cat}^{-1}\ h^{-1}$). Using Pt/TiO_2 photocatalysts deposited on a glass microfiber filter, De La Peña et al. [49] reached CH_4 formation rates over 10 $\mu mol \cdot g_{cat}^{-1}\ h^{-1}$, even though CO was once again obtained as the major product. Tahir and Amin [50] reported the use of a monolithic reactor on which an In/TiO_2 reached CH_4 production rates over 50 $\mu mol \cdot g_{cat}^{-1}\ h^{-1}$ at 100 °C, with CO formation rates of almost 1 $mmol \cdot g_{cat}^{-1}\ h^{-1}$. Also using an internal-illuminated TiO_2-coated honeycomb monolith reactor, Wu et al. [51] reached CH_4 formation rates of 1 $\mu mol \cdot g_{cat}^{-1}\ h^{-1}$. A recent report using core-shell structures based on Cr and Ti oxides by Maroto-Valer et al. [52] inspired in their earlier work [53] obtained CH_4 formation rates over 20 $\mu mol \cdot g_{cat}^{-1}\ h^{-1}$ in a flow reactor similar to the one described in this manuscript.

It must be noted that our results (obtained in gas phase under flow conditions) are very close to the highest reported values to date in the reduction of CO_2 to CH_4 [54–57] with some very distinct differences. The work of Wang et al. uses a pressurized reactor in which the reaction is carried out in liquid phase, while our photocatalysts can operate continuously under ambient temperature and pressure, which are substantially more environmentally friendly conditions. On the other hand, the works of Sorcar et al. [57] and Tahir and Amin [56] use significantly higher light intensities when irradiating the sample (using 300 and 500 W lamps, respectively). In this sense, the use of LED lights in our study corroborates the very high efficiency of our prepared photocatalysts. Furthermore, the very high selectivity of our systems towards CH_4 (>99 %) is yet another advantage to consider when comparing our results with those reported for liquid-phase reactions, in which many different reaction products are obtained [58]. In addition, the 2D-flow reactor designed can be easily scaled up to larger dimensions, thus being an option for a straightforward larger scale application.

In order to better understand the interplay between the TiO_2 phase and the Cu_xO phases and its effect in the overall performance of the resulting photocatalysts, a simple test was devised using a MWCNT film to support the TiO_2 and/or Cu_xO (see Sections 2.2.3, and 2.4). Fig. 8 shows the CH_4 production rates obtained using these samples. It becomes evident that while the MWCNT film alone and the film with deposited Cu (MWCNT film w/ Cu) are completely inactive towards CH_4 production, MWCNT film w/ P25 showed a very small activity of just over 0.06 μmol g $cat^{-1}\ h^{-1}$. The sample containing both P25 and Cu species (MWCNT film w/ P25&Cu) showed a dramatic increase of its

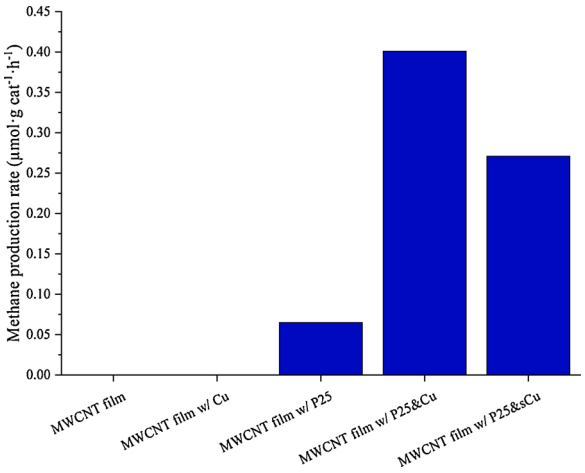

Fig. 8. CH_4 production rates for different species deposited on a MWCNT film.

catalytic activity up to 0.4 μmol g $cat^{-1}\ h^{-1}$ which proved the synergistic effect of having the two species together. Moreover, repetition of the experiment with the same sample but shielding the Cu-deposited side from UV irradiation (MWCNT film w/ P25&sCu) showed a very interesting result. Under these conditions, the CH_4 production rate dropped by 30 % which is a strong indicator that UV irradiation on the Cu side is also of paramount importance, showing that the Cu-derived species are also acting as photocatalysts, not as mere cocatalysts. In this respect, it would appear that while the three-step process described above would still be valid (photoactivation of the TiO_2 phase, charge transport and reduction on a suitable CO_2 adsorbent phase), the third step would also involve light irradiation, which may be indicative of a heterojunction-based phenomenon. In this respect, it becomes mandatory to establish the kind of heterojunction that may be involved in the case of our best performing sample (Cu_1P25).

To better establish the fine interplay between the components of the different photocatalysts, UPS spectra were collected for the best performing sample (Cu_1P25) as well as for the parent P25 material for comparison purposes. This technique measures the kinetic energy of generated photoelectrons from the sample when irradiated with ultraviolet light. While no core-level information is obtained from the spectra, the information it provides on the electronic structure of the valence band is very significant, which makes it a very interesting technique for studying semiconductor-based photocatalysts [59]. Prior to the analyses, the bias voltage was calibrated using a freshly cleaned Ag foil mounted on the sample holder. Fig. 9 shows the obtained full UPS

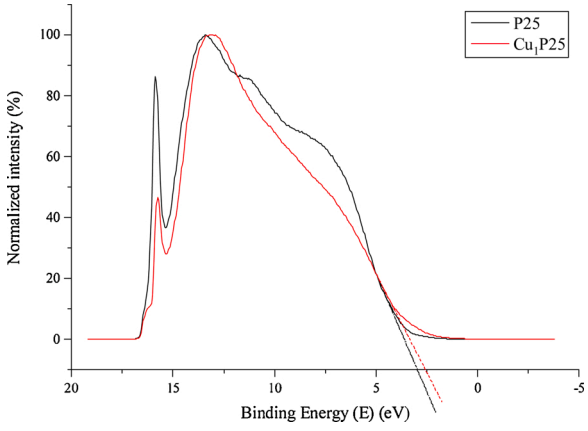

Fig. 9. UPS Spectra collected for samples P25 and Cu_1P25. Dashed lines are presented as a guide to the eye in order to know the position of the valence band maximum (E_{VB}).

spectra of samples P25 and Cu_1P25.

The sharp spike appearing at high binding energies (BE) (or low kinetic energies (KE)) is due to the effect of the flood gun which was used throughout all the experiments in order to ensure that the collected spectra had sufficient resolution to perform an accurate and reliable analysis. Even under these conditions, the cut-off energy obtained using the first derivative of the UPS spectrum was 17.0 eV, in good agreement with other recent reports [60]. At this point, it is important to note that the shape of the UPS spectrum at low BE gives detailed information concerning the density of states (DOS) in the valence band. In other words, it is possible to know the level of electron occupation within the valence band sorted out by energy (i.e. position) within said band. For materials whose performance is directly linked to their valence electrons and their precise binding energy such as semiconductors, it becomes evident that UPS can be crucial to establish the reasons behind the suitability of a given photocatalyst. In this respect, from the analysis of Fig. 9 there is one important feature that must be highlighted. While the density of states for sample P25 at BE values above 5 eV is higher than that of Cu_1P25, the Cu-containing sample shows a higher electron population at lower binding energies (BE 0−5 eV). Considering that these latter energy levels are those located at the top of the valence band (see discussion below), the electrons located in this region will be those closest to the conduction band and thus most active in photocatalytic reactions. This serves to explain the differences in performance observed for both samples. While P25 has a higher electron population at BE above 5 eV than Cu_1P25, the fact that the latter sample has a higher density of states at BE close to the valence band maximum gives it an edge in terms of photocatalytic efficiency for the reaction at hand.

Further analysis of the UPS spectra can also be performed to build the electronic band structure of both samples. The first thing to do in this respect is to establish the valence band maximum (E_{VB}) for both samples, while Maheu et al. [60] suggest using the second derivative of the UPS spectrum, we obtained more accurate results by using the valence band decay extrapolation explained in the literature [61,62]. The dashed lines presented in Fig. 9 show the energy position of the intercept of a straight line fitting the valence band decay and the *x*-axis. From our results, the E_{VB} for P25 and Cu_1P25 samples were 2.9 and 2.5 eV, respectively. This relative positioning of the valence band together with the band-gap energy (E_g) obtained from UV–vis spectra give the overall picture of valence and conduction band positioning, albeit from a relative perspective. To properly describe the electronic structures of the two samples, an absolute measurement of their energy levels was done by using the silver substrate mentioned above (see Experimental section). The E_{VB} maximum for P25 was measured to be 2.9 eV below the Fermi level of silver, while that of Cu_1P25 was 2.5 eV below that same level. Additionally, the work function of this Ag foil was measured to be 4.2 eV. The resulting E_{VB} for P25 and Cu_1P25 are 7.1 and 6.7 eV below the vacuum level, respectively. Using the offset between the E_{VB} of the two samples determined by UPS and with the E_g values determined from the UV–vis spectra (the values were 3.1 and 3.05 eV for samples P25 and Cu_1P25 respectively), the energy level of the conduction band (E_{CB}) may be easily calculated. Thus, the absolute electronic structure for both P and Cu_1P25 is shown in Fig. 10. Note that the energy levels are presented both vs. vacuum and NHE as presented in other reports [18,63].

It must be noted that the absolute band structure for P25 agrees with the literature, and that of the Cu_1P25 presents a band structure in which the electrons promoted to the conduction band have a significantly higher reduction potential, which in turn explains their outstanding photocatalytic efficiency. Considering that the reduction potential of the CO_2/CH_4 and H_2O/H_2 redox pairs is -0.24 V and -0.42 V at pH 7 [18], respectively, it is clear that while both catalysts could perform both reactions under the reaction conditions, the Cu_1P25 largely outperforms its TiO_2-only based counterpart. It becomes clear from looking at the absolute band diagram that sample Cu_1P25 presents a band structure typical of a Z-scheme photocatalyst in which the electrons promoted to the Cu_1P25 conduction band can perform the reduction of CO_2 to CH_4 with very high efficiency.

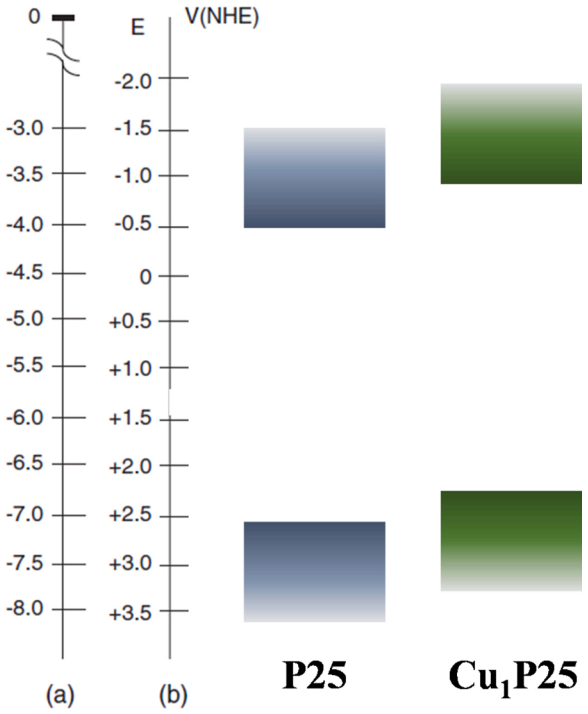

Fig. 10. Absolute positions of the energy bands of photocatalysts P25 and Cu_1P25 with respect to (a) vacuum and (b) electrochemical (Normal Hydrogen Electrode) scales.

3.3. Post-reaction

Concerning the behavior of the photocatalysts after reaction, one aspect that must be brought forward is that all of them were highly stable under the tested reaction conditions in terms of both performance and morphology. In this respect, TEM analyses of the spent samples did not show any noticeable differences with respect to the fresh samples, which is a strong evidence of the robustness of all the TiO_2-based catalysts. While their morphology is very important, the chemical state of the constituents of the photocatalysts deserves special attention given the nature of the catalytic process studied. As Ali et al. [12] highlighted in their study, reduced TiO_2 (RT in their manuscript) is the key ingredient to obtain a system which displays promising performance. In our case, all fresh samples were either white (Cu_1P25) or slightly grey (Cu_1TiO_2C) before reaction, but after reaction all samples turned into different shades of a grey-blue hue that evidenced that changes in the chemical state of the constituents of the catalysts had occurred. UV–vis spectroscopy studies, performed in the samples remaining in the reactor, showed that for all the tested samples absorption of radiation in the visible range took place to a significantly larger extent in the used samples (Fig. 11). In order to ascertain the recoverability of the spent catalysts, we left them on an open bench under atmospheric conditions. After 1 h, the catalysts recovered their initial coloring and their original UV–vis spectra as shown in Fig. 11.

In order to establish this point even more, the fresh P25 and Cu_1P25 samples were placed inside a special sealed vacuum sample holder together with the sample Cu_1P25 obtained immediately after one reaction cycle, and the three samples were analyzed by Raman spectroscopy and XPS in an automated Nexsa spectrometer (see *Experimental* section). In this respect, while the Raman spectra (results not shown) obtained by the irradiation with a 633 nm excitation laser source did not yield any appreciable peaks from Cu phases (due to the low Cu loading), the fundamental modes for both anatase and rutile were clearly observed, as previous reports have also shown [44]. However, the XPS spectra

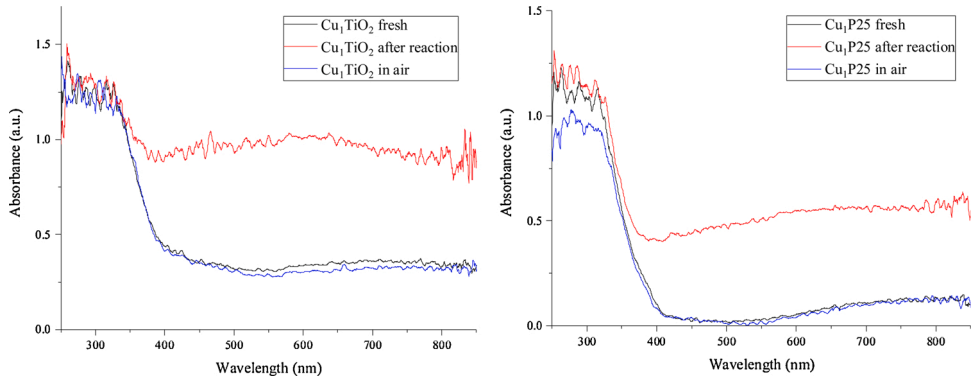

Fig. 11. UV–vis spectra of photocatalysts Cu_1P25 and Cu_1TiO_2 before and after reaction, including a 1 -h open-bench recovery step.

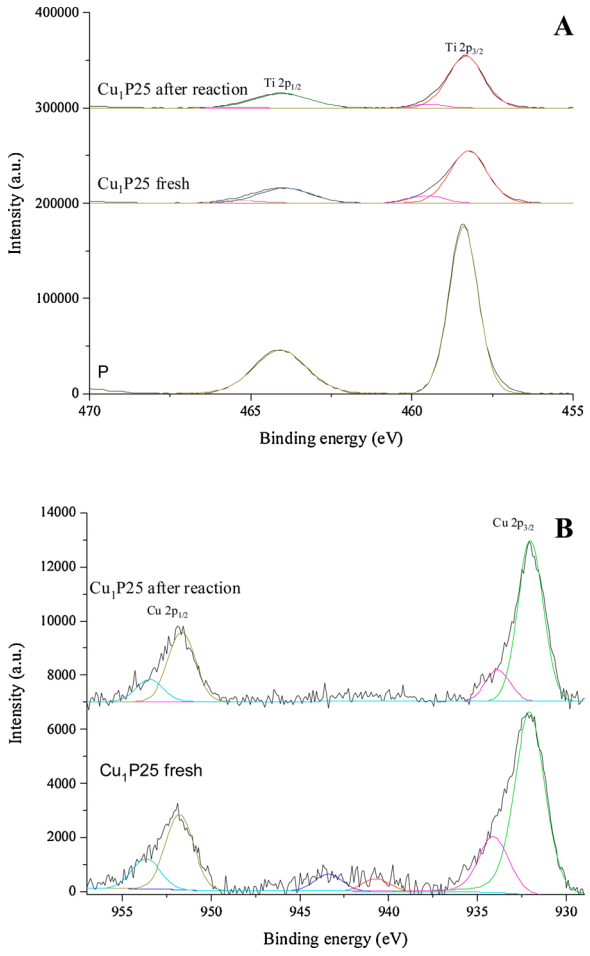

Fig. 12. XPS spectra of sample Cu_1P25 before and after reaction showing the (A) Ti 2p signal and (B) Cu 2p signal. In the case of the Ti 2p signal, the benchmark P25 material is shown for comparison purposes.

(Fig. 12) showed some interesting features. The Ti 2p spectra for the P25 sample showed only one peak centered at 458.3 eV characteristic of pure TiO_2 [64], while for the Cu-containing samples (Cu_1P25 and Cu_1TiO_2) a small additional peak centered 459.5 eV was also found. Considering that no other species are present, this peak may be attributed to the interaction between the metal oxide phases. Furthermore, the Cu 2p scan revealed two distinct signals centered at 932.0 and 933.6 eV, corresponding to Cu_2O and CuO [44,65]. By fitting the peaks using a Lorentzian function, integration of the resulting peaks allowed us to establish the relative amounts of Cu (I) and Cu (II) oxide phases present in both photocatalysts with respect to the total Cu content. The percentage of Cu (I) oxide was 72.1 % for the fresh Cu_1P25 sample, and 84.3 % for the post-reaction sample. This is another evidence of the evolution of the samples during the reaction as shown above by UV analysis, in which reduced Cu_xO phases play a crucial role in the development of efficient CO_2 reduction catalysts.

4. Conclusions

Our study clearly shows that photocatalysts based on the heterojunction of two semiconductors can deliver very interesting results in the formation of CH_4 by the photocatalytic reduction of CO_2 in gas phase. Furthermore, our results highlight the relevance of selecting an appropriate hole scavenger to assist the photocatalyst in reaching the best results possible, which are several orders of magnitude above the best reported results so far. The combination of XRD, TEM, UV–vis, XPS and UPS data have revealed that photocatalysts based on Ti and Cu oxides prepared under carefully controlled conditions present a band diagram which greatly favors the reduction of CO_2 into CH_4. During the reaction, the Cu_xO phases become reduced but are quickly reoxidized under open bench conditions. These systems, prepared following a very simple sol-gel and impregnation procedure are clear examples of highly promising photocatalysts for the green continuous gas-phase synthesis of CH_4 from CO_2. The highly flexible reactor presented in this study must also be highlighted since it is not only simple in its design, but has also great potential in terms of scalability as a result. The crude results obtained in our study were already promising considering those reported in the literature for such a process using similar reactor configurations (1.136 $\mu mol_{CH4} \cdot g_{cat}^{-1} h^{-1}$), but the selection of a proper hole scavenger and the subsequent optimization of its concentration has allowed us to reach CH_4 production rates which are among the best reported irrespective of the reactor and/or conditions (117 $\mu mol_{CH4} \cdot g_{cat}^{-1} h^{-1}$) and using low power LED lighting, which shows the outstanding relevance of our results.

CRediT authorship contribution statement

J. Fernández-Catalá: Conceptualization, Methodology, Investigation, Writing - original draft. **M. Navlani-García:** Conceptualization, Methodology, Investigation, Writing - original draft, Writing - review & editing, Supervision, Funding acquisition. **Á. Berenguer-Murcia:** Conceptualization, Methodology, Writing - review & editing, Supervision. **D. Cazorla-Amorós:** Conceptualization, Methodology, Writing - review & editing, Supervision, Project administration, Funding acquisition.

Declaration of Competing Interest

The authors declare that they have no known competing financial

interests or personal relationships that could have appeared to influence the work reported in this paper.

Acknowledgements

The authors thank the Generalitat Valenciana (PROMETEOII/2018/076) for financial support. MNG gratefully acknowledges Generalitat Valenciana and Plan GenT (CDEIGENT/2018/027) for the postdoctoral grant.

References

[1] P. McKendry, Energy production from biomass (part 1): overview of biomass, Bioresour. Technol. 83 (2002) 37–46, https://doi.org/10.1016/S0960-8524(01)00118-3.
[2] L. Yuan, Y.J. Xu, Photocatalytic conversion of CO_2 into value-added and renewable fuels, Appl. Surf. Sci. 342 (2015) 154–167, https://doi.org/10.1016/j.apsusc.2015.03.050.
[3] M.-Q. Yang, Y.-J. Xu, Photocatalytic conversion of CO_2 over graphene-based composites: current status and future perspective, Nanoscale Horiz. 1 (2016) 185–200, https://doi.org/10.1039/C5NH00113G.
[4] E.V. Kondratenko, G. Mul, J. Baltrusaitis, G.O. Larrazábal, J. Pérez-Ramírez, Status and perspectives of CO_2 conversion into fuels and chemicals by catalytic, photocatalytic and electrocatalytic processes, Energy Environ. Sci. 6 (2013) 3112–3135, https://doi.org/10.1039/C3EE41272E.
[5] J. Schneider, M. Matsuoka, M. Takeuchi, J. Zhang, Y. Horiuchi, M. Anpo, D. W. Bahnemann, Understanding TiO_2 photocatalysis: mechanisms and materials, Chem. Rev. 114 (2014) 9919–9986, https://doi.org/10.1021/cr5001892.
[6] M. Dilla, R. Schlögl, J. Strunk, Photocatalytic CO_2 reduction under continuous flow high-purity conditions: quantitative evaluation of CH_4 formation in the steady-state, ChemCatChem 9 (2017) 696–704, https://doi.org/10.1002/cctc.201601218.
[7] Y. Dong, P. Duchesne, A. Mohan, K.K. Ghuman, P. Kant, L. Hurtado, U. Ulmer, J.Y. Y. Loh, A.A. Tountas, L. Wang, A. Jelle, M. Xia, R. Dittmeyer, G.A. Ozin, Shining light on CO_2: from materials discovery to photocatalyst, photoreactor and process engineering, Chem. Soc. Rev. 49 (2020) 5648–5663, https://doi.org/10.1039/d0cs00597e.
[8] S. Sato, T. Arai, T. Morikawa, Toward solar-driven photocatalytic CO_2 reduction using water as an electron donor, Inorg. Chem. 54 (2015) 5105–5113, https://doi.org/10.1021/ic502766g.
[9] A. Fujishima, K. Honda, Electrochemical photolysis of water at a semiconductor electrode, Nature 238 (1972) 37–38, https://doi.org/10.1038/238037a0.
[10] J. Fernández-Catalá, D. Cazorla-Amorós, Á. Berenguer-Murcia, Facile encapsulation of P25 (TiO_2) in spherical silica with hierarchical porosity with enhanced photocatalytic properties for gas-phase propene oxidation, Appl. Catal. A Gen. 564 (2018) 123–132, https://doi.org/10.1016/j.apcata.2018.07.024.
[11] S.G. Kumar, L.G. Devi, Review on modified TiO_2 photocatalysis under UV/visible light: selected results and related mechanisms on interfacial charge carrier transfer dynamics, J. Phys. Chem. A 115 (2011) 13211–13241, https://doi.org/10.1021/jp204364a.
[12] S. Ali, J. Lee, H. Kim, Y. Hwang, A. Razzaq, J.W. Jung, C.H. Cho, S. In, Sustained, photocatalytic CO_2 reduction to CH_4 in a continuous flow reactor by earth-abundant materials: reduced titania-Cu_2O Z-scheme heterostructures, Appl. Catal. B Environ. 279 (2020), 119344, https://doi.org/10.1016/j.apcatb.2020.119344.
[13] J. García-Aguilar, J. Fernández-Catalá, J. Juan-Juan, I. Such-Basáñez, L. E. Chinchilla, J.J. Calvino-Gámez, D. Cazorla-Amorós, Á. Berenguer-Murcia, Novelty without nobility: outstanding Ni/Ti-SiO_2 catalysts for propylene epoxidation, J. Catal. 386 (2020) 94–105, https://doi.org/10.1016/j.jcat.2020.04.006.
[14] T. Wei, Y.N. Zhu, X. An, L.M. Liu, X. Cao, H. Liu, J. Qu, Defect modulation of Z-scheme TiO_2/Cu_2O photocatalysts for durable water splitting, ACS Catal. 9 (2019) 8346–8354, https://doi.org/10.1021/acscatal.9b01786.
[15] K.C. Christoforidis, P. Fornasiero, Photocatalysis for hydrogen production and CO_2 reduction: the case of copper-catalysts, ChemCatChem 11 (2019) 368–382, https://doi.org/10.1002/cctc.201801198.
[16] M.E. Aguirre, R. Zhou, A.J. Eugene, M.I. Guzman, M.A. Grela, Cu_2O/TiO_2 heterostructures for CO_2 reduction through a direct Z-scheme: protecting Cu_2O from photocorrosion, Appl. Catal. B Environ. 217 (2017) 485–493, https://doi.org/10.1016/j.apcatb.2017.05.058.
[17] J. Low, C. Jiang, B. Cheng, S. Wageh, A.A. Al-Ghamdi, J. Yu, A review of direct Z-scheme photocatalysts, Small Methods 1 (2017) 1–21, https://doi.org/10.1002/smtd.201700080.
[18] W. Zhang, A.R. Mohamed, W.J. Ong, Z-scheme photocatalytic systems for carbon dioxide reduction: where are we now? Angew. Chem. Int. Ed. 59 (2020) 22894–22915, https://doi.org/10.1002/anie.201914925.
[19] P. Zhou, J. Yu, M. Jaroniec, All-solid-state Z-scheme photocatalytic systems, Adv. Mater. 26 (2014) 4920–4935, https://doi.org/10.1002/adma.201400288.
[20] R. Leary, A. Westwood, Carbonaceous nanomaterials for the enhancement of TiO_2 photocatalysis, Carbon 49 (2011) 741–772, https://doi.org/10.1016/j.carbon.2010.10.010.
[21] K. Woan, G. Pyrgiotakis, W. Sigmund, Photocatalytic carbon-nanotube–TiO_2 composites, Adv. Mater. 21 (2009) 2233–2239, https://doi.org/10.1002/adma.200802738.
[22] M. Ouzzine, M.A. Lillo-Ródenas, A. Linares-Solano, Carbon nanofibres as substrates for the preparation of TiO_2 nanostructured photocatalysts, Appl. Catal. B 127 (2012) 291–299, https://doi.org/10.1016/j.apcatb.2012.08.029.
[23] N.M. Dimitrijevic, B.K. Vijayan, O.G. Poluektov, T. Rajh, K.A. Gray, H. He, P. Zapol, Role of water and carbonates in photocatalytic transformation of CO_2 to CH_4 on titania, J. Am. Chem. Soc. 133 (2011) 3964–3971, https://doi.org/10.1021/ja108791u.
[24] C. Amatore, J.M. Savéant, Mechanism and kinetic characteristics of the electrochemical reduction of carbon dioxide in media of low proton availability, J. Am. Chem. Soc. 103 (1981) 5021–5023, https://doi.org/10.1021/ja00407a008.
[25] I.A. Shkrob, T.W. Marin, H. He, P. Zapol, Photoredox reactions and the catalytic cycle for carbon dioxide fixation and methanogenesis on metal oxides, J. Phys. Chem. C 116 (2012) 9450–9460, https://doi.org/10.1021/jp300122v.
[26] L. Liu, Y. Li, Understanding the reaction mechanism of photocatalytic reduction of CO_2 with H_2O on TiO_2-based photocatalysts: a review, Aerosol Air Qual. Res. 14 (2) (2014) 453–469, https://doi.org/10.4209/aaqr.2013.06.0186.
[27] K. Guo, X. Zhu, L. Peng, Y. Fu, R. Ma, X. Lu, F. Zhang, W. Zhu, M. Fan, Boosting photocatalytic CO_2 reduction over a covalent organic framework decorated with ruthenium nanoparticles, Chem. Eng. J. 405 (2021), 127011, https://doi.org/10.1016/j.cej.2020.127011.
[28] J. Albo, G. García, Enhanced visible-light photoreduction of CO_2 to methanol over Mo_2C/TiO_2 surfaces in an optofluidic microreactor, React. Chem. Eng. 6 (2021) 304–312, https://doi.org/10.1039/d0re00376j.
[29] M. Salaices, B. Serrano, H.I. De Lasa, Experimental evaluation of photon absorption in an aqueous TiO_2 slurry reactor, Chem. Eng. J. 90 (2002) 219–229, https://doi.org/10.1016/S1385-8947(02)00037-2.
[30] S. Mazzanti, S. Cao, K. ten Brummelhuis, A. Völkel, J. Khamrai, D.I. Sharapa, S. Youk, T. Heil, N.V. Tarakina, V. Strauss, I. Ghosh, B. König, M. Oschatz, M. Antonietti, A. Savateev, All-organic Z-scheme photoreduction of CO_2 with water as the donor of electrons and protons, Appl. Catal. B Environ. 285 (2021), 119773, https://doi.org/10.1016/j.apcatb.2020.119773.
[31] S. Meng, C. Chen, X. Gu, H. Wu, Q. Meng, J. Zhang, S. Chen, X. Fu, D. Liu, Efficient photocatalytic H_2 evolution, CO_2 reduction and N_2 fixation coupled with organic synthesis by cocatalyst and vacancies engineering, Appl. Catal. B Environ. 285 (2021), 119789, https://doi.org/10.1016/j.apcatb.2020.119789.
[32] B. Mei, A. Pougin, J. Strunk, Influence of photodeposited gold nanoparticles on the photocatalytic activity of titanate species in the reduction of CO_2 to hydrocarbons, J. Catal. 306 (2013) 184–189, https://doi.org/10.1016/j.jcat.2013.06.027.
[33] F. Galli, M. Compagnoni, D. Vitali, C. Pirola, C.L. Bianchi, A. Villa, L. Prati, I. Rossetti, CO_2 photoreduction at high pressure to both gas and liquid products over titanium dioxide, Appl. Catal. B Environ. 200 (2017) 386–391, https://doi.org/10.1016/j.apcatb.2016.07.038.
[34] K. Li, X. An, K.H. Park, M. Khraisheh, J. Tang, A critical review of CO_2 photoconversion: catalysts and reactors, Catal. Today 224 (2014) 3–12, https://doi.org/10.1016/j.cattod.2013.12.006.
[35] H. Kim, R.C.Y. Auyeung, M. Ollinger, G.P. Kushto, Z.H. Kafafi, A. Piqué, Laser-sintered mesoporous TiO_2 electrodes for dye-sensitized solar cells, Appl. Phys. A Mater. Sci. Process. 83 (2006) 73–76, https://doi.org/10.1007/s00339-005-3449-0.
[36] Y. Li, W.N. Wang, Z. Zhan, M.H. Woo, C.Y. Wu, P. Biswas, Photocatalytic reduction of CO_2 with H_2O on mesoporous silica supported Cu/TiO_2 catalysts, Appl. Catal. B Environ. 100 (2010) 386–392, https://doi.org/10.1016/j.apcatb.2010.08.015.
[37] M. Dilla, A.E. Becerikli, A. Jakubowski, R. Schlögl, S. Ristig, Development of a tubular continuous flow reactor for the investigation of improved gas-solid interaction in photocatalytic CO_2 reduction on TiO_2, Photochem. Photobiol. Sci. 18 (2019) 314–318, https://doi.org/10.1039/c8pp00518d.
[38] J. Fernández-Catalá, L. Cano-Casanova, M.Á. Lillo-Ródenas, Á. Berenguer-Murcia, D. Cazorla-Amorós, Synthesis of TiO_2 with hierarchical porosity for the photooxidation of propene, Molecules 22 (2017) 2243, https://doi.org/10.3390/molecules22122243.
[39] J. Fernández-Catalá, Á. Berenguer-Murcia, D. Cazorla-Amorós, Study of MWCNT dispersion effect in TiO_2-MWCNT composites for gas-phase propene photooxidation, Mater. Res. Bull. 134 (2021), 111089, https://doi.org/10.1016/j.materresbull.2020.111089.
[40] J. Fernández-Catalá, M. Navlani-García, P. Verma, Á. Berenguer-Murcia, K. Mori, Y. Kuwahara, H. Yamashita, D. Cazorla-Amorós, Photocatalytically-driven H_2 production over Cu/TiO_2 catalysts decorated with multi-walled carbon nanotubes, Catal. Today 364 (2021) 182–189, https://doi.org/10.1016/j.cattod.2020.05.032.
[41] A.W. Dweydari, C.H.B. Mee, Work function measurements on (100) and (110) surfaces of silver, Phys. Status Solidi A 27 (1975) 223–230, https://doi.org/10.1002/pssa.2210270126.
[42] B. Li, H. Cao, G. Yin, Y. Lu, J. Yin, Cu_2O@reduced graphene oxide composite for removal of contaminants from water and supercapacitors, J. Mater. Chem. 21 (2011) 10645–10648, https://doi.org/10.1039/c1jm12135a.
[43] K. Wang, X. Dong, C. Zhao, X. Qian, Y. Xu, Facile synthesis of Cu_2O/CuO/RGO nanocomposite and its superior cyclability in supercapacitor, Electrochim. Acta 152 (2015) 433–442, https://doi.org/10.1016/j.electacta.2014.11.171.
[44] P.A. Bharad, A.V. Nikam, F. Thomas, C.S. Gopinath, CuOx-TiO_2 composites: electronically integrated nanocomposites for solar hydrogen generation, ChemistrySelect 3 (2018) 12022–12030, https://doi.org/10.1002/slct.201802047.
[45] X. Qiu, M. Miyauchi, K. Sunada, M. Minoshima, M. Liu, Y. Lu, D. Li, Y. Shimodaira, Y. Hosogi, Y. Kuroda, K. Hashimoto, Hybrid Cu_xO / TiO_2 nanocomposites as risk-reduction materials in indoor, ACS Nano 6 (2012) 1609–1618, https://doi.org/10.1021/nn2045888.
[46] K. Chaudhary, M. Trivedi, D.T. Masram, A. Kumar, G. Kumar, A. Husain, N.P. Rath, A highly active copper catalyst for the hydrogenation of carbon dioxide to formate

under ambient conditions, Dalton Trans. 49 (2020) 2994–3000, https://doi.org/10.1039/c9dt04662c.
[47] W. Liao, P. Liu, Methanol synthesis from CO_2 hydrogenation over a potassium-promoted $Cu_xO/Cu(111)$ ($x \leq 2$) model surface: rationalizing the potential of potassium in catalysis, ACS Catal. 10 (2020) 5723–5733, https://doi.org/10.1021/acscatal.9b05226.
[48] Y. Li, W.N. Wang, Z. Zhan, M.H. Woo, C.Y. Wu, P. Biswas, Photocatalytic reduction of CO_2 with H_2O on mesoporous silica supported Cu/TiO_2 catalysts, Appl. Catal. B Environ. 100 (2010) 386–392, https://doi.org/10.1016/j.apcatb.2010.08.015.
[49] M. Tasbihi, F. Fresno, U. Simon, I.J. Villar-García, V. Pérez-Dieste, C. Escudero, V. A. de la Peña O'Shea, On the selectivity of CO_2 photoreduction towards CH_4 using Pt/TiO_2 catalysts supported on mesoporous silica, Appl. Catal. B Environ. 239 (2018) 68–76, https://doi.org/10.1016/j.apcatb.2018.08.003.
[50] M. Tahir, N.S. Amin, Photocatalytic CO_2 reduction and kinetic study over In/TiO_2 nanoparticles supported microchannel monolith photoreactor, Appl. Catal. A Gen. 467 (2013) 483–496, https://doi.org/10.1016/j.apcata.2013.07.056.
[51] Z. Xiong, Z. Lei, S. Ma, X. Chen, B. Gong, Y. Zhao, J. Zhang, C. Zheng, J.C.S. Wu, Photocatalytic CO_2 reduction over V and W codoped TiO_2 catalyst in an internal-illuminated honeycomb photoreactor under simulated sunlight irradiation, Appl. Catal. B Environ. 219 (2017) 412–424, https://doi.org/10.1016/j.apcatb.2017.07.078.
[52] J.Z.Y. Tan, F. Xia, M.M. Maroto-Valer, Raspberry-like microspheres of core–shell $Cr_2O_3@TiO_2$ nanoparticles for CO_2 photoreduction, ChemSusChem. 12 (2019) 5246–5252, https://doi.org/10.1002/cssc.201901712.
[53] W.A. Thompson, C. Perier, M.M. Maroto-Valer, Systematic study of sol-gel parameters on TiO_2 coating for CO_2 photoreduction, Appl. Catal. B Environ. 238 (2018) 136–146, https://doi.org/10.1016/j.apcatb.2018.07.018.
[54] R. Li, Q. Luan, C. Dong, W. Dong, W. Tang, G. Wang, Y. Lu, Light-facilitated structure reconstruction on self-optimized photocatalyst TiO_2@BiOCl for selectively efficient conversion of CO_2 to CH_4, Appl. Catal. B Environ. 286 (2021), 119832, https://doi.org/10.1016/j.apcatb.2020.119832.
[55] S. Ali, M.C. Flores, A. Razzaq, S. Sorcar, C.B. Hiragond, H.R. Kim, Y.H. Park, Y. Hwang, H.S. Kim, H. Kim, E.H. Gong, J. Lee, D. Kim, S. In, Gas phase photocatalytic CO2 reduction, "A brief overview for benchmarking", Catalysts 9 (2019) 727, https://doi.org/10.3390/catal9090727.
[56] M. Tahir, N.A.S. Amin, Photocatalytic reduction of carbon dioxide with water vapors over montmorillonite modified TiO_2 nanocomposites, Appl. Catal. B Environ. 142 (2013) 512–522, https://doi.org/10.1016/j.apcatb.2013.05.054.
[57] S. Sorcar, Y. Hwang, C.A. Grimes, S. In, Highly enhanced and stable activity of defect-induced titania nanoparticles for solar light-driven CO_2 reduction into CH_4, Mater. Today 20 (2017) 507–515, https://doi.org/10.1016/j.mattod.2017.09.005.
[58] J. Wang, J. Ma, Q. Zhang, Y. Chen, L. Hong, B. Wang, J. Chen, H. Jing, New heterojunctions of CN/TiO_2 with different band structure as highly efficient catalysts for artificial photosynthesis, Appl. Catal. B Environ. 285 (2021), 119781, https://doi.org/10.1016/j.apcatb.2020.119781.
[59] R.H. Williams, G.P. Srivastava, I.T. McGovern, Photoelectron spectroscopy of solids and their surfaces, Rep. Prog. Phys. 43 (1980) 1357–1414.
[60] C. Maheu, L. Cardenas, E. Puzenat, P. Afanasiev, C. Geantet, UPS and UV spectroscopies combined to position the energy levels of TiO_2 anatase and rutile nanopowders, Phys. Chem. Chem. Phys. 20 (2018) 25629–25637, https://doi.org/10.1039/c8cp04614j.
[61] S.A. Chambers, T. Droubay, T.C. Kaspar, M. Gutowski, Experimental determination of valence band maxima for $SrTiO_3$, TiO_2, and SrO and the associated valence band offsets with Si (001), J. Vac. Sci. Technol. B Microelectron. Nanometer Struct. 22 (2004) 2205–2215, https://doi.org/10.1116/1.1768525.
[62] A. Giampietri, G. Drera, L. Sangaletti, Band alignment at heteroepitaxial perovskite oxide interfaces. Experiments, methods, and perspectives, Adv. Mater. Interfaces 4 (2017), 1700144, https://doi.org/10.1002/admi.201700144.
[63] B. Wang, X. Xiao, T. Chen, Perovskite photovoltaics: a high-efficiency newcomer to the solar cell family, Nanoscale 6 (2014) 12287–12297, https://doi.org/10.1039/c4nr04144e.
[64] R.P. Netterfield, P.J. Martin, C.G. Pacey, W.G. Sainty, Ion-assisted deposition of mixed TiO_2-SiO_2 films, J. Appl. Phys. 66 (1989) 1805.
[65] Z. Jin, C. Liu, K. Qi, X. Cui, Photo-reduced Cu/CuO nanoclusters on TiO_2 nanotube arrays as highly efficient and reusable catalyst, Sci. Rep. 7 (2017) 1–9, https://doi.org/10.1038/srep39695.